Magnetic-field-induced quadrupole coupling in the nuclear magnetic resonance of noble-gas atoms and molecules

Pekka Manninen,[1,2,*] Juha Vaara,[1,†] and Pekka Pyykkö[3,‡]
[1]*Laboratory of Physical Chemistry, Department of Chemistry, P.O. Box 55 (A.I. Virtasen aukio 1), FIN-00014 University of Helsinki, Finland*
[2]*NMR Research Group, Department of Physical Sciences, P.O. Box 3000, FIN-90014 University of Oulu, Finland*
[3]*Laboratory for Instruction in Swedish, Department of Chemistry, P.O. Box 55 (A.I. Virtasen aukio 1), FIN-00014 University of Helsinki, Finland*
(Received 10 May 2004; published 5 October 2004)

An analytic response theory formulation for the leading-order magnetic field-induced and field-dependent quadrupole splitting in nuclear magnetic resonance spectra is presented and demonstrated with first-principles calculations for ^{21}Ne, ^{36}Ar, and ^{83}Kr in noble gas atoms. The case of molecules was studied for ^{33}S in the sulphur hexafluoride molecule, as well as for $^{47/49}$Ti, ^{91}Zr, and ^{177,179}Hf in group(IV) tetrahalides. According to our calculations, the hitherto experimentally unknown field-induced quadrupole splitting in molecules rises to 10^2 Hz for ^{177,179}Hf nuclei in HfF_4 and 10^1 Hz for $^{47/49}$Ti in $TiCl_4$, and is hence of observable magnitude.

DOI: 10.1103/PhysRevA.70.043401 PACS number(s): 33.25.+k, 31.15.−p

I. INTRODUCTION

A nonvanishing average electric-field gradient (EFG) at the site of an atomic nucleus, possessing an electric quadrupole moment, leads to quadrupole splittings in the nuclear magnetic resonance (NMR) spectrum, when the nuclear site symmetry is lower than cubic (or tetrahedral). This interaction appears in the effective NMR spin Hamiltonian as a term, bilinear in the nuclear spin [1]. Meersmann and Haake [2] measured the spectra of ^{131}Xe in the gaseous and isotropic liquid phases as a function of the external magnetic flux density B_0, and observed a field-induced quadrupole splitting. Salsbury and Harris [3] proposed a qualitative explanation of the effect in terms of a magnetic-field-induced diamagnetic deformation of the electron cloud of the Xe atom. They suggested both linear and quadratic dependences on B_0. However, the requirement of time-reversal invariance forbids, in closed-shell systems, the existence of energy terms quadratic in the nuclear spin **I** and scaling with an odd power in B_0. Proportionality of the quadrupole coupling to an odd power in B_0 requires the presence of minimally three components of **I** in the corresponding energy term, and such combinations have not been found necessary in the analysis of any NMR experiment so far [4]. In Ref. [4], a theoretical analysis and quantitative *ab initio* calculations were presented for the case of field-induced and -dependent quadrupole splitting in atomic ^{131}Xe. The effect has not yet been observed in molecules, or in atoms other than Xe.

The magnetic-field dependence of related NMR properties have been investigated. The case of nuclear magnetic shielding has been treated computationally in Refs. [5–9]. In particular, the sole experimental observation of field-dependent chemical shifts, for ^{59}Co in Co(III) complexes [10], was supported by the calculations of Ref. [9]. The field dependence of the indirect spin-spin coupling was investigated through model calculations in Ref. [11].

In this paper, we present an analytical response theory [12] formulation of the field-dependent quadrupole coupling, generalized for molecules of arbitrary symmetry and tested using *ab initio* Hartree-Fock (HF) self-consistent-field (SCF), multiconfigurational SCF (MCSCF), as well as density-functional-theory (DFT) calculations. We estimate the quadrupole splitting of ^{21}Ne, ^{36}Ar, and ^{83}Kr nuclei in noble-gas atoms, ^{33}S in SF_6, ^{47}Ti and ^{49}Ti in TiF_4 and $TiCl_4$, ^{91}Zr in ZrF_4, as well as ^{177}Hf and ^{179}Hf in HfF_4. The field-independent quadrupole splitting is absent in these systems due to the high site symmetry, which is spherical in the noble-gas atoms, O_h in SF_6, and T_d in the group IV tetrahalides. In Ref. [4], both the field dependence quartic in the external field, as well as the pseudoquadrupole (second-order magnetic hyperfine) contributions to the field-dependent quadrupole coupling, were found to be negligible. For this reason, we consider in this work only the true quadrupole interaction having a quadratic magnetic-field dependence. We assume that the molecular structure is independent of the magnetic field.

II. THEORY

A. Field-induced quadrupole interaction

The Cartesian $\epsilon\tau$ component of the quadrupole coupling tensor $\mathcal{B}$ can be written as the first derivative of a Taylor series expansion of the perturbed molecular energy E, with respect to the bilinear product of nuclear spin components [13],

$$\mathcal{B}_{\epsilon\tau} = \left.\frac{1}{2\pi}\frac{dE}{dI_\epsilon I_\tau}\right|_{\mathbf{I}=\mathbf{0}} = \mathcal{B}^{(0)}_{\epsilon\tau} + \frac{1}{2!}\sum_{\gamma\delta}\mathcal{B}^{(2)}_{\epsilon\tau,\gamma\delta}B_{0,\gamma}B_{0,\delta} + \cdots, \tag{1}$$

where $\mathcal{B}^{(0)}$ is the field-independent quadrupole coupling tensor, and

*Email address: manninen@chem.helsinki.fi.
†Corresponding author. Email address: jvaara@chem.helsinki.fi.
‡Email address: Pekka.Pyykko@helsinki.fi.

$$\mathcal{B}^{(2)}_{\epsilon\tau,\gamma\delta} = \frac{1}{2\pi} \left. \frac{\partial^3 E}{\partial I_\epsilon I_\tau \partial B_{0,\gamma} \partial B_{0,\delta}} \right|_{\mathbf{I}=\mathbf{B}_0=\mathbf{0}} \tag{2}$$

corresponds to the leading, quadratic, field-induced contribution.

In terms of the Breit-Pauli molecular Hamiltonian [14], consideration of the perturbation-theoretical energy expressions with both a quadratic dependence on the field and a quadratic dependence on the nuclear spin coordinates gives rise to the leading field-induced, true quadrupole coupling contributions

$$\mathcal{B}^{(2),\mathrm{dia}}_{\epsilon\tau,\gamma\delta} = \frac{1}{2\pi} P_{\gamma\delta} \langle\langle h^{\mathrm{NQCC}}_{\epsilon\tau}; h^{\mathrm{SUSC}}_{B_0^2,\gamma\delta} \rangle\rangle_0 = \frac{1}{\pi} \langle\langle h^{\mathrm{NQCC}}_{\epsilon\tau}; h^{\mathrm{SUSC}}_{B_0^2,\gamma\delta} \rangle\rangle_0, \tag{3}$$

$$\mathcal{B}^{(2),\mathrm{para}}_{\epsilon\tau,\gamma\delta} = \frac{1}{2\pi} \frac{P_{\gamma\delta}}{2!} \langle\langle h^{\mathrm{NQCC}}_{\epsilon\tau}; h^{\mathrm{OZ}}_{B_0,\gamma}, h^{\mathrm{OZ}}_{B_0,\delta} \rangle\rangle_{0,0} = \frac{1}{2\pi} \langle\langle h^{\mathrm{NQCC}}_{\epsilon\tau}; h^{\mathrm{OZ}}_{B_0,\gamma}, h^{\mathrm{OZ}}_{B_0,\delta} \rangle\rangle_{0,0}. \tag{4}$$

In these expressions, the abbreviations denote the nuclear quadrupole coupling (NQCC), diamagnetic susceptibility (SUSC), and the orbital Zeeman (OZ) interaction,

$$H^{\mathrm{NQCC}}_K = \sum_{\epsilon\tau} h^{\mathrm{NQCC}}_{K,\epsilon\tau} I_{K,\epsilon} I_{K,\tau},$$

$$h^{\mathrm{NQCC}}_{K,\epsilon\tau} = -\frac{1}{2} \frac{Q_K}{I_K(2I_K-1)} F_{K,\epsilon\tau}, \tag{5}$$

$$F_{K,\epsilon\tau} = \sum_i \frac{3 r_{iK,\epsilon} r_{iK,\tau} - \delta_{\epsilon\tau} r^2_{iK}}{r^5_{iK}}, \tag{6}$$

$$H^{\mathrm{SUSC}}_{B_0^2} = \sum_{\epsilon\tau} h^{\mathrm{SUSC}}_{\epsilon\tau} B_{0,\epsilon} B_{0,\tau},$$

$$h^{\mathrm{SUSC}}_{\epsilon\tau} = \frac{1}{8} \sum_i (\delta_{\epsilon\tau} r^2_{iO} - r_{iO,\epsilon} r_{iO,\tau}), \tag{7}$$

$$H^{\mathrm{OZ}}_{B_0} = \sum_\epsilon h^{\mathrm{OZ}}_\epsilon B_{0,\epsilon}, \quad h^{\mathrm{OZ}}_\epsilon = \frac{1}{2} \sum_i \ell_{iO,\epsilon}, \tag{8}$$

where the Coulomb gauge

$$\mathbf{A}_0 = \frac{1}{2} \mathbf{B}_0 \times \mathbf{r}_{iO} \tag{9}$$

has been used for the magnetic vector potential $\mathbf{A}_0$. In these formulas, $\mathbf{r}_{iK}$ and $\mathbf{r}_{iO}$ are the position vectors of electron i with respect to nucleus K and the gauge origin O, respectively, and ℓ_{iO} is the angular momentum with respect to O. The symbol $P_{\gamma\delta}$ denotes a sum of both permutations of the indices γ and δ and $\mathbf{F}$ is the EFG operator. Here and in the following, linear, quadratic, and cubic response functions, $\langle\langle A;B\rangle\rangle_0$, $\langle\langle A;B,C\rangle\rangle_{0,0}$, and $\langle\langle A;B,C,D\rangle\rangle_{0,0,0}$, correspond to standard second-, third-, and fourth-order perturbation theory expressions, respectively, featuring time-independent perturbations A to D [12]. The latter equalities in Eqs. (3) and (4) follow from the symmetry upon, in the former case, the interchange of the subscripts γ and δ of the h^{SUSC} operator and the permutation of the two h^{OZ} operators for the latter equation.

Partial first-order, scalar relativistic (SR) corrections to the field-induced quadrupole coupling contributions are provided by

$$\mathcal{B}^{(2),\mathrm{dia/mvd}}_{\epsilon\tau,\gamma\delta} = \frac{1}{\pi} \langle\langle h^{\mathrm{NQCC}}_{\epsilon\tau}; h^{\mathrm{SUSC}}_{B_0^2,\gamma\delta}, h^{\mathrm{mv}} + h^{\mathrm{Dar}} \rangle\rangle_{0,0}, \tag{10}$$

$$\mathcal{B}^{(2),\mathrm{para/mvd}}_{\epsilon\tau,\gamma\delta} = \frac{1}{2\pi} \langle\langle h^{\mathrm{NQCC}}_{\epsilon\tau}; h^{\mathrm{OZ}}_{B_0,\gamma}, h^{\mathrm{OZ}}_{B_0,\delta}, h^{\mathrm{mv}} + h^{\mathrm{Dar}} \rangle\rangle_{0,0,0}, \tag{11}$$

where the mass velocity (mv) and one-electron Darwin (Dar) operators are

$$h^{\mathrm{mv}} = -\frac{1}{8} \alpha^2 \sum_i \nabla^4_i, \tag{12}$$

$$h^{\mathrm{Dar}} = \frac{\pi}{2} \alpha^2 \sum_K Z_K \sum_i \delta(\mathbf{r}_{iK}). \tag{13}$$

In these equations, α denotes the fine-structure constant, $\delta(\mathbf{r}_{iK})$ is the Dirac delta function, and Z_K is the charge of nucleus K. The mvd correction was shown to be numerically important in the study of ^{131}Xe in Ref. [4].

B. Relation to experiment

In the high-field approximation, the NMR spin Hamiltonian corresponding to the quadrupole interaction is $H_{\mathrm{NMR}} \approx \frac{3}{2} \mathcal{B}_{ZZ} I^2_Z = \Delta_Z \mathcal{B} I^2_Z$, where $\Delta_Z \mathcal{B}$ is the anisotropy of $\boldsymbol{\mathcal{B}}$ in the Z direction of the external magnetic field. This Hamiltonian gives rise to a symmetric spectrum with $2I$ peaks for a nucleus with the spin quantum number I, with the distance of the peaks equaling $3|\mathcal{B}_{ZZ}|$. Hence, the total width of the spectral pattern is

$$w = (2I-1)3|\mathcal{B}_{ZZ}| = (2I-1)2|\Delta_Z \mathcal{B}|. \tag{14}$$

We carry out calculations for the expressions (3) and (4) as well as their SR corrections (10) and (11) in the case of noble-gas atoms and molecules. The special case of atoms is simple, as the calculations of $\Delta_Z \mathcal{B}$ can be directly carried out in the laboratory frame. Furthermore, Eqs. (4) and (11) do not contribute in atoms as the reference state $|0\rangle$ is an eigenstate of $h^{\mathrm{OZ}}_{B_0}$.

Applying Eq. (1), the anisotropy in the laboratory-fixed (X,Y,Z) frame is

$$\Delta_Z\mathcal{B} = \mathcal{B}_{ZZ} - \frac{1}{2}(\mathcal{B}_{XX} + \mathcal{B}_{YY}) = \frac{1}{2}\left[\mathcal{B}^{(2)}_{ZZ,ZZ} - \frac{1}{2}(\mathcal{B}^{(2)}_{XX,ZZ} + \mathcal{B}^{(2)}_{YY,ZZ})\right]B_0^2 \equiv \frac{1}{2}\Delta_Z\mathcal{B}^{(2)}B_0^2, \quad (15)$$

since $\Delta_Z\mathcal{B}^{(0)}$ vanishes for the nuclear site symmetries relevant presently. For molecules tumbling freely in the isotropic liquid or gas phase, the anisotropy of $\boldsymbol{\mathcal{B}}^{(2)}$ in the direction of the field can be expressed in the molecule-fixed (x,y,z) frame as [15]

$$\begin{aligned}\Delta_Z\mathcal{B}^{(2)} = [&4\mathcal{B}^{(2)}_{xx,xx} - 2\mathcal{B}^{(2)}_{xx,yy} - 2\mathcal{B}^{(2)}_{xx,zz} + 3\mathcal{B}^{(2)}_{xy,xy} \\ &+ 3\mathcal{B}^{(2)}_{xy,yx} + 3\mathcal{B}^{(2)}_{xz,xz} + 3\mathcal{B}^{(2)}_{xz,zx} + 3\mathcal{B}^{(2)}_{yx,xy} + 3\mathcal{B}^{(2)}_{yx,yx} \\ &- 2\mathcal{B}^{(2)}_{yy,xx} + 4\mathcal{B}^{(2)}_{yy,yy} - 2\mathcal{B}^{(2)}_{yy,zz} + 3\mathcal{B}^{(2)}_{yz,yz} + 3\mathcal{B}^{(2)}_{yz,zy} \\ &+ 3\mathcal{B}^{(2)}_{zx,xz} + 3\mathcal{B}^{(2)}_{zx,zx} + 3\mathcal{B}^{(2)}_{zy,yz} + 3\mathcal{B}^{(2)}_{zy,zy} - 2(\mathcal{B}^{(2)}_{zz,xx} \\ &+ \mathcal{B}^{(2)}_{zz,yy} - 2\mathcal{B}^{(2)}_{zz,zz})]/30. \end{aligned} \quad (16)$$

In both O_h and T_d point-group symmetries, $\mathcal{B}^{(2)}_{xx,xx} = \mathcal{B}^{(2)}_{yy,yy} = \mathcal{B}^{(2)}_{zz,zz}$. The components with two identical instances of both the nuclear spin and the external magnetic-field indices are equal (e.g., $\mathcal{B}^{(2)}_{xx,yy} = \mathcal{B}^{(2)}_{yy,zz}$). In addition, the components with two different indices for the spin and the same two indices for the external magnetic field are mutually equal (e.g., $\mathcal{B}^{(2)}_{xy,xy} = \mathcal{B}^{(2)}_{yz,yz}$).

III. COMPUTATIONAL DETAILS

The geometry of SF_6 ($r_{SF} = 155.68$ pm) was obtained from Ref. [16]. Tetrahedral geometries of the group IV tetrafluorides were optimized using DFT with the BECKE-PERDEW86 exchange-correlation functional [17] and the GAUSSIAN98 software [18]. Energy-consistent, relativistic small-core pseudopotential (PPs) [19] were used for the transition-metal atoms, while large-core PPs [20] were employed for F and Cl. The corresponding Gaussian valence basis sets were of the (6*s* 5*p* 3*d*) and (2*s* 3*p*) types, correspondingly. The bond lengths obtained were $r_{TiF} = 175.93$ pm, $r_{TiCl} = 218.36$ pm, $r_{ZrF} = 193.66$ pm, and $r_{HfF} = 193.45$ pm. For the tetrahedral TiF_4 and $TiCl_4$, the experimental (electron diffraction) bond lengths are 176 pm [21] and 217 pm [22], respectively, while 190 pm was reported both for ZrF_4 and HfF_4 [23].

HF, MCSCF, and DFT calculations of the field-induced quadrupole coupling were carried out using the DALTON quantum chemistry software [24]. Values of 10.155 fm^2 [25], 11.0 fm^2 [26], 25.9 fm^2 [25], and −6.78 fm^2 [25] were used for quadrupole moments of ^{21}Ne, ^{36}Ar, ^{82}Kr, and ^{33}S, respectively. For group IV nuclei, the quadrupole moments [25] of 30.2 fm^2 and 24.7 fm^2 for ^{47}Ti and ^{49}Ti, −17.6 fm^2 for ^{91}Zr, as well as 336.5 fm^2 and 379.2 fm^2 for ^{177}Hf and ^{179}Hf, respectively, were used. The nuclear spin quantum numbers of the presently studied nuclei are $I = \frac{3}{2}$ for ^{21}Ne and ^{33}S, $I = \frac{5}{2}$ for ^{47}Ti and ^{91}Zr, $I = \frac{7}{2}$ for ^{49}Ti and ^{177}Hf, and $I = \frac{9}{2}$ for ^{83}Kr and ^{179}Hf. In addition, $I = 2$ for a short-lived excited state of the ^{36}Ar isotope [26], and this nucleus is only included in the present work for the purpose of investigating systematic trends down the noble-gas series.

Contracted Gaussian one-particle basis sets were used as detailed in Table I. A basis-set convergence study is reported for the noble gases and SF_6. Results for the group IV tetrahalides are only presented with the final, converged sets listed in Table I.

The DFT calculations for all the systems used the three-parameter hybrid Becke-Lee-Yang-Parr (B3LYP) [34] exchange-correlation functional. MCSCF wave functions of complete active space (CASSCF) [35] and restricted active space (RASSCF) [36] types were used for the noble-gas atoms as given in Table II. CASSCF calculations were also carried out for SF_6, with active orbitals chosen to involve ten electrons in five active orbitals in A_g, two active orbitals in each of B_{1u}, B_{2u}, and B_{3u}, and one active orbital in each of B_{1g}, B_{2g}, and B_{3g} irreps of the computational, Abelian D_{2h} point-group symmetry. This choice yields 5.0×10^5 Slater determinants in the wave function. The HIV21 basis set was used with the CASSCF calculations.

IV. RESULTS AND DISCUSSION

A. Noble-gas atoms

The calculated factors $\Delta_Z\mathcal{B}^{(2)}/B_0^2$ and the total widths of the quadrupole pattern in the spectrum, $w/B_0^2 = (2I-1)|\Delta_Z\mathcal{B}^{(2)}|$, Eqs. (15) and (14), respectively, are presented for ^{21}Ne, ^{36}Ar, and ^{83}Kr in Table III. The corresponding values for ^{131}Xe, obtained from Refs. [2] and [4], are also included. Figure 1 illustrates a schematic spectrum for the example case of $I = \frac{3}{2}$. The basis-set dependence in the HF calculations of $\Delta_Z\mathcal{B}^{(2),\mathrm{dia}}$ is most pronounced in Ne, where the difference between the HII and HIII results is close to 20%. At the same time, corresponding changes of 3% and −0.3% occur in Ar and Kr, respectively. The step from HIII to the HIV level leads to a few percent decrease in the absolute value of this contribution in both Ne, Ar, and Kr. Whereas the decontraction of the HIV set, upon reaching the HIVu level, does not cause an appreciable effect, the addition of diffuse *s*, *p*, *d*, and *f* functions on top of the HIVu set (HIVu0*n*) gives rise to a significant increase in the absolute value of $\Delta_Z\mathcal{B}^{(2),\mathrm{dia}}$ in Ar and Kr, and a much less pronounced effect on Ne. Two sets of diffuse *spdf* functions provide a practical convergence in all the atoms studied. Each of the supplemented sets of tight functions, applied on top of the HIVu02 set, alters the absolute value by maximally 1−2%, and three additional sets are sufficient for saturating the basis set. Despite the facts that the additional *g* function cannot change the HF results at all for Ne and Ar, where the highest occupied angular momentum value in the ground state is $l_{max} = 1$, and the influence is not large even for Kr ($l_{max} = 2$), the *g* function was employed in the correlated MCSCF calculations.

According to the comparison presented in Ref. [8], the single-reference RAS-II wave function, featuring single and double excitations into a large active atomic orbital space, is well-converged with respect to the electron correlation treat-

TABLE I. Basis sets used in the calculations. Spherical Gaussian functions used. The data are given in the primitive/contracted notation. Only the innermost orbitals of each type, 1*s* and 2*p*, were contracted. Elements from the same row in the Periodic Table obtain the same polarization exponents according to the IGLO scheme [27].

Element	H$_{II}$	H$_{III}$	H$_{IV}$	Saturated[a]
Noble-gas atoms				
Ne[b]	[9*s* 5*p* 1*d*/5*s* 4*p* 1*d*]	[11*s* 7*p* 2*d*/7*s* 6*p* 2*d*]	[11*s* 7*p* 3*d* 1*f*/8*s* 7*p* 3*d* 1*f*]	[16*s* 12*p* 8*d* 6*f* 1*g*]
Ar[b]	[11*s* 7*p* 2*d*/7*s* 6*p* 2*d*]	[12*s* 8*p* 3*d*/8*s* 7*p* 3*d*]	[12*s* 8*p* 4*d* 2*f*/9*s* 8*p* 4*d* 2*f*]	[17*s* 13*p* 9*d* 7*f* 1*g*]
Kr[c]	[16*s* 13*p* 10*d*/11*s* 10*p* 10*d*]	[16*s* 13*p* 11*d*/12*s* 11*p* 11*d*]	[16*s* 13*p* 12*d* 2*f*/13*s* 12*p* 12*d* 2*f*]	[21*s* 18*p* 17*d* 7*f* 1*g*]
SF_6 *molecule*				
S[b]	[11*s* 7*p* 2*d*/7*s* 6*p* 2*d*]	[12*s* 8*p* 3*d*/8*s* 7*p* 3*d*]	[12*s* 8*p* 4*d* 2*f*/9*s* 8*p* 4*d* 2*f*]	[15*s* 11*p* 6*d* 4*f* 1*g*]
F[b]	[9*s* 5*p* 1*d*/5*s* 4*p* 1*d*]	[11*s* 7*p* 2*d*/7*s* 6*p* 2*d*]	[11*s* 7*p* 3*d* 1*f*/8*s* 7*p* 3*d* 1*f*]	[14*s* 10*p* 5*d* 3*f* 1*g*]
Saturated basis sets for MX_4 *molecules*				
Ti[d]	Zr[e]	Hf[f]	F	Cl[g]
[20*s* 17*p* 14*d* 6*f*]	[24*s* 18*p* 18*d* 6*f* 1*g*]	[25*s* 19*p* 19*d* 13*f* 5*g*]	[15*s* 11*p* 7*d* 5*f*][h] [14*s* 10*p* 6*d* 4*f*][i]	[16*s* 12*p* 8*d* 6*f*]

[a]Sets obtained by supplementing the fully uncontracted H$_{II}$(H$_{IV}$u) basis by *m* high-exponent (tight) and *n* diffuse *s*, *p*, *d*, and *f* functions in order to saturate the basis in the both core and valence regions. The new *m*(*n*) exponents were obtained by multiplying (dividing) the largest (smallest) existing exponent by 3. Further *g*-type polarization functions (exponents 2.983 [28], 1.007 [29], and 0.7395 [30] for Ne and F, Ar and S, and Kr, respectively) were supplemented on top of the converged H$_{IV}$u*mn* sets, giving the final uncontracted H$_{IV}$u32+*g* sets for the noble gases and H$_{IV}$u21+*g* for SF_6 (with only one tight function added to the *d* and *f* subspaces in SF_6).

[b]Sets based on the primitive sets by Huzinaga [31] and supplemented with polarization functions as well as contracted by Kutzelnigg *et al.* [27] (at the H$_{II}$-H$_{IV}$ levels).

[c]The underlying (16*s* 13*p* 8*d*) set is from Ref. [32]. The polarization exponents of the two (H$_{II}$), three (H$_{III}$), and four (H$_{IV}$) *d*-type polarization functions were obtained by successive division by a factor of 3, starting from the most diffuse existing function. The exponents of the *f*-type functions in the H$_{IV}$ set are (0.426,0.142).

[d]The underlying (16*s* 10*p* 8*d*) set is taken from Ref. [32] and supplied with two *f*-type polarization functions with exponents identical to those used for Kr (footnote c), three sets of tight *spdf* functions, and diffuse functions as follows: 1*s*, 4*p*, 3*d*, and 1*f*. The exponents of the tight and diffuse functions were obtained as in footnote a.

[e]The underlying (20*s* 14*p* 11*d*) set is from Ref. [32] and supplied with two *f*-type polarization functions with exponents (0.327,0.109), three sets of tight *spdf* functions, and diffuse functions as follows: 1*s*, 1*p*, 4*d*, and 1*f*. The exponents of the tight and diffuse functions were obtained as in footnote a. A further polarization *g* function (exponent 0.210513 [33]) was also added.

[f]The underlying (22*s* 16*p* 13*d* 8*f*) set is from Ref. [32] and supplied with two *g*-type polarization functions with exponents (0.32628, 0.15706 [33]), two sets of tight *spdfg* functions, and diffuse functions as follows: 1*s*, 1*p*, 4*d*, 3*f*, and 1*g*. The exponents of the tight and diffuse functions were obtained as in footnote a.

[g]Based on the H$_{IV}$ set as in footnote b, and complemented to H$_{IV}$u31 as in footnote a.

[h]Used for TiF_4 and ZrF_4; based on the H$_{IV}$ set as in footnote b, and complemented to H$_{IV}$u31 as in footnote a.

[i]Used for HfF_4; based on the H$_{IV}$ set as in footnote b, and complemented to H$_{IV}$u21 as in footnote a.

ment, at least in the case of the magnetic-field dependence of nuclear shielding in noble-gas atoms. On the other hand, the present results obtained using the single-reference RAS-I and the corresponding multireference CAS wave functions, are very close to each other. Consequently, the role of the higher than double excitations can be assumed to be small, and hence the RAS-II results should be very reliable. In a further comparison with DFT, it is seen that B3LYP overestimates electron correlation effects.

The effect of SR corrections is negligible for Ne but corresponds to 2% and 10% of the total field-induced quadrupole coupling in Ar and Kr, respectively, at the RAS-II/H$_{IV}$u32+*g* level. While the SR correction is sensitive to the choice of the basis, it nevertheless converges at our biggest basis-set levels. Electron correlation is less important, and B3LYP overestimates the absolute magnitude of the relativistic correction, too. Perturbational spin-orbit (SO) interaction corrections, if one would proceed in analogy with the perturbational calculation of the relativistic effects in nuclear shielding (see, e.g., Ref. [37]), appear to $O(\alpha^4)$, which renders the SO contribution small for Kr and the lighter elements.

In the last column of Table II, the results are presented for the field-induced non-relativistic (NR) EFG, free from the nuclear factors (the quadrupole moment *Q* and the spin quantum number *I*). Hence, a comparison of the electronic response property is possible down the noble-gas column of the Periodic Table. The contribution of the electron cloud scales roughly as $Z^{1.5}$ as a function of the nuclear charge, *Z*.

The present, scalar relativistically corrected calculations are obtained using a rigorous electron correlation treatment nearly at the basis-set limit, and give widths, in units of mHz/T^2, of the field-induced quadrupole coupling patterns equal to 0.66, 1.72, 5.15, and 14.84 [4] for ^{21}Ne, ^{36}Ar, ^{83}Kr,

TABLE II. Multiconfiguration self-consistent-field wave functions used in the calculations of the noble-gas atoms.

System	Identifier	WF type[a]	N_e [b]	Active space[c]	N_{SD} [d]
Ne	RAS-I	SR	8	$2s\ 2p \rightarrow 3s\ 3p\ 3d$	253
	CAS	MR	8	$2s\ 2p \rightarrow 3s\ 3p\ 3d$	64 331
	RAS-II	SR	10	$1s\ 2s\ 2p \rightarrow 3s\ 3p\ 3d\ 4s\ 4p\ 4d\ 4f\ 5s\ 5p$	4042
Ar	RAS-I	SR	8	$3s\ 3p \rightarrow 3d$	87
	CAS	MR	8	$3s\ 3p \rightarrow 3d$	2016
	RAS-II	SR	16	$2s\ 2p\ 3s\ 3p \rightarrow 3d\ 4s\ 4p\ 4d\ 4f\ 5s\ 5p$	7529
Kr	RAS-I	SR	8	$4s\ 4p \rightarrow 4d$	87
	CAS	MR	8	$4s\ 4p \rightarrow 4d$	2016
	RAS-II	SR	26	$3s\ 3p\ 3d\ 4s\ 4p \rightarrow 4d\ 4f\ 5s\ 5p\ 5d\ 5f\ 6s\ 6p$	32 165

[a]Specification of single- (SR) or multireference (MR) wave function.
[b]Number of correlated electrons.
[c]Correlated atomic orbitals (AOs). In the case of a SR wave function, single and double excitations from the occupied to the virtual AOs contained within the active space are allowed. The MR (CAS) wave function corresponds to full configuration interaction in the active AO space.
[d]Number of Slater determinants contained in the wave function.

and ^{131}Xe, respectively. These results correspond to 0.29, 0.76, 2.30, and 6.63 Hz in the magnetic field of an NMR spectrometer with 900 MHz resonance frequency for ^{1}H(B_0 = 21.14 T) The effect on ^{21}Ne is most probably too small to be observed, and experiments with ^{36}Ar are not feasible due its very short lifetime. Instead, the total splitting of ^{83}Kr is about one-half of the previous, experimentally observed splitting of 14 mHz/T^2 in ^{131}Xe [2], hinting at the possibility of experimental detection.

B. Sulfur hexafluoride

For ^{33}S in SF_6, the calculated $\Delta_Z\mathcal{B}^{(2),\mathrm{dia}}$ and $\Delta_Z\mathcal{B}^{(2),\mathrm{para}}$ coefficients [Eq. (16) broken into the contributions arising from Eqs. (3) and (4), respectively] as well as their scalar relativistic corrections [Eqs. (10) and (11)] are presented in Table IV. The total dia- and para-anisotropy coefficients are of the same sign, when converted to the laboratory frame using Eq. (16). Both terms give contributions of the same order of magnitude. In the molecule-fixed frame, the tensor components with all four indices equal, e.g., $\mathcal{B}_{xx,xx}$, have oppositely signed dia- and para-contributions, while the components with crossed spin and field indices, $\mathcal{B}_{xy,xy}$, etc., exhibit the same sign for the two contributions. The transformation into the laboratory frame for the anisotropy of $\boldsymbol{\mathcal{B}}$ weighs the different tensor components in a different way. The resulting, somewhat counterintuitively identical signs of the dia- and para-contributions for ^{33}S in SF_6 cannot be generalized to other systems (*vide infra*).

Particularly, the para-contribution is sensitive to the basis-set quality. Differences of over 50% are observed between the smallest and the largest basis sets used. The step between HII and HIII has the most pronounced effect, which implies that polarized triple-zeta basis sets such as HII may not be adequate for this property. Successive addition of two tight sets and one diffuse set of primitives on top of the uncontracted HIvu set, at the HIvu21 level, saturates the *spdf* basis. The effect of the additional *g* functions on top of the HIvu21 set (HIvu21+*g*) is small in all contributions. Due to their minor importance as well as practical computational limitations, the *g* functions were omitted in the CASSCF calculations.

Electron correlation effects are significant especially for the dia-contribution, showing ~20% differences between the HF and DFT levels. For the para-contribution, DFT gives systematically a few percent larger values than HF, and ~12% larger than CASSCF. Of the methods used presently, DFT is likely to perform the best for SF_6, since the CASSCF calculation is not sufficient for adequate treatment of dynamical correlation in this electron-rich system. The current active space is the largest feasible, balanced choice for SF_6 that we can make.

As the present system contains only relatively light nuclei, the SR corrections, dia/mvd and para/mvd, turn out to be unimportant, being smaller by two orders of magnitude than the corresponding leading contributions. The SR corrections of both dia- and para-contributions are dependent on the basis set, but converge by the HIvu21 level. The para/mvd contribution is 20% larger than the corresponding dia/mvd term, and both share the positive sign of the NR contributions.

The total $\Delta_Z\mathcal{B}^{(2)}$ is 0.7–0.9 mHz/T^2 with our best basis sets, at the different levels of theory used presently. Hence, based on the B3LYP/HIvu21+*g* results, we are able to predict a width of 1.47 mHz/T^2 for the field-induced ^{33}S quadrupole pattern in SF_6. This corresponds to 0.66 Hz in a 900 MHz spectrometer. Since the linewidth of the ^{33}S NMR spectrum of SF_6 is ~1 Hz in a liquid sample [38], the experimental observation of the field-induced quadrupole splitting is challenging for this system, with the currently available field strengths. The field-induced EFG of ^{33}S in SF_6 is between the values obtained for Ar and Kr atoms.

TABLE III. Calculated coefficients $\Delta_Z\mathcal{B}^{(2)}/B_0^2$ of the magnetic-field-induced anisotropy of the NMR quadrupole coupling tensors of noble-gas atoms ^{21}Ne, ^{36}Ar, and ^{83}Kr, and the widths of the field-induced splitting patterns, w. The terms of $\Delta_Z\mathcal{B}^{(2)}/B_0^2$ and w/B_0^2 in mHz/T^2, w(900 MHz) in Hz.

Nucleus	Theory	Basis set	dia[a]	dia/mvd[b]	Total[c]	w/B_0^2 [d]	w(900 MHz)[e]	F_{ZZ}/B_0^2 [f]
^{21}Ne	HF	HII	−0.2788	−0.0011	−0.2799	0.5598	0.25	1.29
		HIII	−0.3353	−0.0017	−0.3369	0.6738	0.30	1.55
		HIV	−0.3216	−0.0018	−0.3234	0.5469	0.29	1.49
		HIVu	−0.3216	−0.0018	−0.3234	0.6469	0.29	1.49
		HIVu01	−0.3355	−0.0019	−0.3275	0.6749	0.30	1.55
		HIVu02	−0.3349	−0.0019	−0.3368	0.6736	0.30	1.55
		HIVu03	−0.3349	−0.0019	−0.3368	0.6736	0.30	1.55
		HIVu12	−0.3331	−0.0021	−0.3341	0.6703	0.30	1.54
		HIVu22	−0.3282	−0.0022	−0.3304	0.6609	0.30	1.52
		HIVu32	−0.3280	−0.0022	−0.3302	0.6604	0.30	1.52
		HIVu32+g	−0.3280	−0.0022	−0.3302	0.6604	0.30	1.52
	B3LYP	HIVu32+g	−0.3716	−0.0027	−0.3742	0.7485	0.33	1.72
	CAS	HIVu32+g	−0.3255	−0.0022	−0.3278	0.6555	0.29	1.51
	RAS-I	HIVu32+g	−0.3255	−0.0022	−0.3267	0.6534	0.29	1.50
	RAS-II	HIVu32+g	−0.3265	−0.0022	−0.3287	0.6575	0.29	1.51
^{36}Ar	HF	HII	−0.4470	−0.0066	−0.4536	1.3607	0.61	3.82
		HIII	−0.4620	−0.0084	−0.4704	1.4111	0.63	3.95
		HIV	−0.4487	−0.0090	−0.4578	1.3733	0.61	3.84
		HIVu	−0.4487	−0.0090	−0.4578	1.3733	0.61	3.84
		HIVu01	−0.5760	−0.0121	−0.5881	1.7643	0.79	4.93
		HIVu02	−0.5800	−0.0121	−0.5922	1.7766	0.79	4.96
		HIVu03	−0.5805	−0.0121	−0.5926	1.7779	0.80	4.96
		HIVu12	−0.5794	−0.0129	−0.5923	1.7760	0.79	4.95
		HIVu22	−0.5751	−0.0136	−0.5888	1.7663	0.79	4.92
		HIVu32	−0.5730	−0.0135	−0.5866	1.7596	0.79	4.90
		HIVu32+g	−0.5730	−0.0135	−0.5866	1.7596	0.79	4.90
	B3LYP	HIVu32+g	−0.6279	−0.0154	−0.6433	1.9300	0.86	5.37
	CAS	HIVu32+g	−0.5710	−0.0127	−0.5837	1.7512	0.78	4.88
	RAS-I	HIVu32+g	−0.5710	−0.0128	−0.5838	1.7513	0.78	4.88
	RAS-II	HIVu32+g	−0.5592	−0.0133	−0.5725	1.7176	0.76	4.78
^{83}Kr	HF	HII	−0.5652	−0.0430	−0.6082	4.8654	2.17	12.31
		HIII	−0.5632	−0.0485	−0.6118	4.8942	2.19	12.27
		HIV	−0.5497	−0.0521	−0.6019	4.8150	2.15	11.98
		HIVu	−0.5496	−0.0542	−0.6039	4.8310	2.15	11.98
		HIVu01	−0.5779	−0.0571	−0.6350	5.0800	2.27	12.59
		HIVu02	−0.5783	−0.0571	−0.6354	5.0831	2.27	12.60
		HIVu03	−0.5783	−0.0571	−0.6354	5.0830	2.27	12.60
		HIVu12	−0.5767	−0.0585	−0.6316	5.0813	2.27	12.57
		HIVu22	−0.5761	−0.0600	−0.6360	5.0882	2.27	12.55
		HIVu32	−0.5758	−0.0601	−0.6359	5.0872	2.27	12.55
		HIVu32+g	−0.5764	−0.0613	−0.6358	5.0862	2.27	12.54
	B3LYP	HIVu32+g	−0.6365	−0.0671	−0.7034	5.6286	2.52	13.87
	CAS	HIVu32+g	−0.5458	−0.0575	−0.6033	4.8263	2.16	11.89
	RAS-I	HIVu32+g	−0.5475	−0.0576	−0.6051	4.8410	2.16	11.93
	RAS-II	HIVu32+g	−0.5833	−0.0679	−0.6441	5.1525	2.30	12.71
^{131}Xe	HF [4]	HIVu32	5.9395	1.4699	7.4094	14.819	6.62	23.87
	RAS-III [4]		5.9577	1.4631	7.4208	14.842	6.63	23.95
	Exp. [2]					14		

[a]Equation (3).
[b]Equation (10).
[c]Sum of the dia and dia+mvd contributions.
[d]The distance between the outermost lines of the quadrupole splitting pattern as a function of magnetic field.
[e]The value of the quantity of footnote d in the magnetic field of an NMR magnet with 900 MHz proton resonance frequency.
[f]The electronic contribution only, expressed in terms of the traceless, nonrelativistic field-dependent EFG tensor, $F_{ZZ}/B_0^2=\frac{1}{2}F^{(2),\mathrm{dia}}_{ZZ,ZZ}$, where $F^{(2),\mathrm{dia}}_{\epsilon\tau,\gamma\delta}=2\langle\langle F_{\epsilon\tau};h^{\mathrm{SUSC}}_{\gamma\delta}\rangle\rangle_0$, in atomic units.

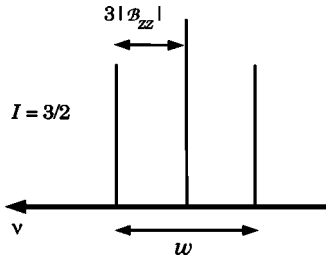

FIG. 1. Schematic quadrupole splitting pattern for a nucleus with $I=\frac{3}{2}$. For a general nuclear spin quantum number I, the spectrum of total width w consists of $2I$ equidistant peaks, the distance of which is $3|\mathcal{B}_{ZZ}|=2|\Delta_Z\mathcal{B}|$.

C. Group IV tetrahalides

Results for $^{47/49}$Ti, ^{91}Zr, and $^{177/179}$Hf in the tetrahedral group IV tetrafluorides as well as $TiCl_4$ are presented in Table V. For these systems, the contributions from Eqs. (3) and (4) now have opposite signs. The para-contribution is clearly the dominant one, being almost two orders of magnitude larger than the dia-contribution.

While both terms are strongly dependent on the basis, we only report the results obtained using our saturated basis sets. The role of electron correlation is significant in all the systems and in both the dia- and para-contributions. DFT gives a systematically larger absolute value for the field-induced quadrupole coupling. The differences range from 6% (HfF_4) to over 70% ($TiCl_4$) in the dia-contribution and from 13% ($TiCl_4$) to roughly 30% (the other systems) in the decisive para-contribution.

The SR corrections are of the same sign with the corresponding NR contributions in ZrF_4 and HfF_4, and small for $TiCl_4$ and $TiCl_4$. The dia/mvd term is smaller in magnitude than the para/mvd correction, in analogy with the NR contributions. The dia/mvd corrections provide a smaller than 1% correction to the total value in HfF_4, and are vanishingly small in the lighter compounds. The para/mvd correction is more significant and ranges from roughly 1% to 10% of the total field-induced coupling for $TiFl_4$ to HfF_4, correspondingly.

With DFT/B3LYP, we obtain the total widths of the field-induced quadrupole coupling patterns of 19/11, 38/22, 14, and 350/310 mHz/T^2 for $^{47/49}TiF_4$, $^{47/49}TiCl_4$, $^{91}ZrF_4$, and $^{177/179}HfF_4$, respectively. It is seen that while the quadrupole moments of the two Ti isotopes on one hand and the two Hf isotopes on the other are of roughly the same magnitude, the lighter isotope of the same element exhibits a larger field-induced splitting due to its smaller spin quantum number I. While the number of peaks in the spectrum increases with I, the separation of the peaks decreases proportional to I^{-2}.

The fluorides of the present study typically form crystalline solids at the temperatures relevant for NMR experiments. In these solids, the site symmetry of the central group IV element is not tetrahedral. Consequently, the currently discussed effect may in practice only become visible in special gas-phase studies for these systems. On the other hand, $TiCl_4$ is a liquid at room temperature, with narrow accessible linewidths. This, combined with the width of the field-induced quintet of 17 Hz in a 900 MHz spectrometer, makes $^{47}TiCl_4$ a promising candidate for an experimental observation of this phenomenon.

V. CONCLUSIONS

We have presented an analytical response theory formulation for the leading, quadratic external magnetic-field depen-

TABLE IV. Calculated coefficients $\Delta_Z\mathcal{B}^{(2)}/B_0^2$ of the magnetic-field-induced anisotropy of the NMR quadrupole coupling tensors of ^{33}S in SF_6, and the widths of the field-induced splitting patterns, w. The terms of $\Delta_Z\mathcal{B}^{(2)}/B_0^2$ and w/B_0^2 in mHz/T^2, w(900 MHz) in Hz. See the footnotes in Table III. No entry means cubic response is not yet available for DFT in DALTON. In this case HF values for the para/mvd corrections were used in the total field-induced splitting patterns.

Theory	Basis set	dia	para[a]	dia/mvd	para/mvd[b]	Total[c]	w/B_0^2	w(900 MHz)	F_{ZZ}/B_0^{2}[d]
HF	HII	0.3747	0.1880	0.0054	0.0140	0.5872	1.1743	0.53	3.90
	HIII	0.3578	0.3725	0.0063	0.0071	0.7437	1.4873	0.67	5.07
	HIV	0.3459	0.4211	0.0066	0.0083	0.7822	1.5643	0.70	5.32
	HIVu	0.3459	0.4211	0.0066	0.0083	0.7822	1.5643	0.70	5.32
	HIVu21	0.3471	0.4301	0.0073	0.0096	0.7956	1.5912	0.70	5.39
	HIVu21+g	0.3471	0.4301	0.0073	0.0097	0.7924	1.5849	0.71	5.39
B3LYP	HII	0.2974	0.2513	0.0027		0.5655	1.1310	0.50	3.81
	HIII	0.2885	0.3810	0.0038		0.6732	1.3465	0.60	4.64
	HIV	0.2804	0.4302	0.0041		0.7147	1.4294	0.64	4.93
	HIVu	0.2804	0.4302	0.0041		0.7147	1.4294	0.64	4.93
	HIVu21	0.2816	0.4389	0.0048		0.7253	1.4506	0.65	5.00
	HIVu21+g	0.2815	0.4378	0.0048		0.7337	1.4675	0.66	4.99
CAS	HIVu21	0.5033	0.3839	−0.0223	0.0206	0.8819	1.7638	0.78	6.15

[a]Equation (4).
[b]Equation (11).
[c]Sum of the dia, para, dia+mvd, and para+mvd contributions.
[d]As in footnote f of Table III, but including also the para contribution with $F^{(2),\mathrm{para}}_{\epsilon\tau,\gamma\delta}=\langle\langle F_{\epsilon\tau};h^{\mathrm{OZ}}_{\gamma},h^{\mathrm{OZ}}_{\delta}\rangle\rangle_{0,0}$.

TABLE V. Calculated coefficients $\Delta_Z\mathcal{B}^{(2)}/B_0^2$ of the magnetic-field-induced anisotropy of the NMR quadrupole coupling tensors of $^{47/49}$Ti, ^{91}Zr, and $^{177/179}$Hf, in group IV tetrahalides, and the widths of the field-induced splitting patterns, w. The terms of $\Delta_Z\mathcal{B}^{(2)}/B_0^2$ and w/B_0^2 in mHz/T^2, w(900 MHz) in Hz. Results with converged basis sets (see Table I) are reported. See footnotes in Table III and footnote d in Table IV.

Molecule	Theory	dia	para	dia/mvd	para/mvd	Total	w/B_0^2	w(900 MHz)	F_{ZZ}/B_0^2
$^{47}TiF_4$	HF	−0.0403	3.0839	−0.0009	−0.0455	2.9970	11.9882	5.36	−15.80
	B3LYP	−0.0632	4.8329	−0.0001		4.7215	18.8861	8.44	−24.76
$^{49}TiF_4$	HF	−0.0157	1.2011	−0.0004	−0.0177	1.1672	7.0035	3.13	
	B3LYP	−0.0246	1.8823	0.0000		1.8404	11.0425	4.94	
$^{47}TiCl_4$	HF	−0.0349	8.6930	0.0026	−0.2688	8.3918	33.5674	15.00	−44.94
	B3LYP	−0.1372	10.0072	0.0045		9.6058	38.4230	17.17	−51.23
$^{49}TiCl_4$	HF	−0.0136	3.3856	0.0037	−0.1047	3.2710	19.6261	8.77	
	B3LYP	−0.0534	3.8974	0.0043		3.7434	22.4604	10.04	
$^{91}ZrF_4$	HF	0.1320	−2.3596	0.0136	−0.0262	−2.2401	8.9604	4.00	−19.84
	B3LYP	0.1402	−3.6361	0.0062		−3.5158	14.0633	6.29	−31.14
$^{177}HfF_4$	HF	−2.8162	39.3487	−0.9100	4.0675	39.6902	238.1410	106.43	−35.74
	B3LYP	−3.0010	58.6582	−0.8007		58.9240	353.5442	158.00	−54.45
$^{179}HfF_4$	HF	−1.8517	25.8729	−0.5980	2.6745	26.0974	208.7793	93.30	
	B3LYP	−1.9732	38.5694	−0.7058		38.5650	308.5197	137.88	

dence of the nuclear magnetic resonance (NMR) quadrupole coupling tensor, based on the Breit-Pauli electronic Hamiltonian. The discussion of the true quadrupole coupling to this order in the field strength as well as its partial scalar relativistic correction, is extended to molecules from a previously published treatment of the atomic case [4]. Calculations are carried out for ^{21}Ne, ^{36}Ar, and ^{83}Kr in noble-gas atoms, as well as $^{33}SF_6$, MF_4 (M=$^{47/49}$Ti, ^{91}Zr, $^{177/179}$Hf), and $^{47/49}TiCl_4$ molecules. Hartree-Fock self-consistent field, multiconfigurational self-consistent-field, and density-functional-theory reference states were used with analytical linear and nonlinear response theory as well as nearly complete basis sets. The NMR nuclei in the present systems possess either spherical (atoms), octahedral (SF_6), or tetrahedral (MF_4, MCl_4) site symmetry, hence eliminating the field-independent quadrupole coupling and leaving only the field-induced contributions. We predict the hitherto experimentally unobserved quadrupole splitting pattern of completely magnetic-field-induced origin, in the experimentally most promising candidates, $^{47}TiCl_4$ and $^{177}HfF_4$, to have the widths of 38 mHz/T^2 and 350 mHz/T^2, respectively. Furthermore, the field-induced splitting possibly also is observable in the spectrum of atomic ^{83}Kr, the width of the nonet being 5 mHz/T^2 in this case.

ACKNOWLEDGMENTS

We thank Trygve Helgaker (Oslo) and Pawel Sałek (Stockholm) for providing the pre-release DFT version of the DALTON software, as well as Jani Saunavaara, Juhani Lounila, and Jukka Jokisaari (Oulu) for useful discussions. Economic support has been received from Jenny and Antti Wihuri as well as Magnus Ehrnrooth Foundations (P.M.), Vilho, Yrjö, and Kalle Väisälä and Tauno Tönninki Foundations (P.M.), The Academy of Finland (J.V., benefiting also of the Academy project number 206001 of Professor J. Jokisaari as well as P.P., projects 200903 and 206102), and the Emil Aaltonen Foundation (J.V.). The computational resources were partially provided by the Center for Scientific Computing, Espoo, Finland.

[1] A. Abragam, *The Principles of Nuclear Magnetism* (Oxford University Press, Oxford, 1960); C. P. Slichter, *Principles of Magnetic Resonance*, 3rd ed. (Springer-Verlag, Berlin, 1992).
[2] T. Meersmann and M. Haake, Phys. Rev. Lett. **81**, 1211 (1998).
[3] F. R. Salsbury, Jr., and R. A. Harris, J. Chem. Phys. **109**, 8338 (1998).
[4] J. Vaara and P. Pyykkö, Phys. Rev. Lett. **86**, 3268 (2001).
[5] N. F. Ramsey, Phys. Rev. A **1**, 1320 (1970).
[6] D. M. Doddrell, D. T. Pegg, and M. R. Bendall, Aust. J. Chem. **32**, 1 (1979).
[7] A. Boucekkine, G. Boucekkine-Yaker, M. Nait-Achour, and G. Berthier, J. Mol. Struct.: THEOCHEM **166**, 109 (1988).
[8] J. Vaara, P. Manninen, and J. Lounila, Chem. Phys. Lett. **372**, 750 (2003).
[9] P. Manninen and J. Vaara, Phys. Rev. A **69**, 022503 (2004).
[10] M. R. Bendall and D. M. Doddrell, J. Magn. Reson. (1969-1992) **33**, 659 (1979).
[11] W. T. Raynes and S. J. Stevens, Magn. Reson. Chem. **30**, 124 (1992).

[12] J. Olsen and P. Jørgensen, J. Chem. Phys. **82**, 3235 (1985); in *Modern Electronic Structure Theory, Part II*, edited by D. R. Yarkony (World Scientific, Singapore, 1995).
[13] A SI-based atomic unit system is used throughout the work.
[14] R. E. Moss, *Advanced Molecular Quantum Mechanics* (Chapman and Hall, London, 1973); J. E. Harriman, *Theoretical Foundations of Electron Spin Resonance* (Academic, New York, 1978); R. McWeeny, *Methods of Molecular Quantum Mechanics*, 2nd ed. (Academic, London, 1992).
[15] D. P. Craig and T. Thirunamachandran, *Molecular Quantum Electrodynamics: An Introduction to Radiation-Molecule Interactions* (Academic Press, London, 1984).
[16] A. A. Ischenko, J. D. Ewbank, and L. Schaefer, J. Phys. Chem. **98**, 4287 (1994).
[17] A. D. Becke, Phys. Rev. A **38**, 3098 (1988); J. P. Perdew, Phys. Rev. B **33**, 8822 (1986).
[18] M. J. Frisch, G. W. Trucks, H. B. Schlegel, G. E. Scuseria, M. A. Robb, J. R. Cheeseman, V. G. Zakrzewski, J. A. Montgomery, R. E. Stratmann, J. C. Burant, S. Dapprich, J. M. Millam, A. D. Daniels, K. N. Kudin, M. C. Strain, O. Farkas, J. Tomasi, V. Barone, M. Cossi, R. Cammi, B. Mennucci, C. Pomelli, C. Adamo, S. Clifford, J. Ochterski, G. A. Petersson, P. Y. Ayala, Q. Cui, K. Morokuma, D. K. Malick, A. D. Rabuck, K. Raghavachari, J. B. Foresman, J. Cioslowski, J. V. Ortiz, B. B. Stefanov, G. Liu, A. Liashenko, P. Piskorz, I. Komaromi, R. Gomperts, R. L. Martin, D. J. Fox, T. Keith, M. A. Al-Laham, C. Y. Peng, A. Nanayakkara, C. Gonzalez, M. Challacombe, P. M. W. Gill, B. G. Johnson, W. Chen, M. W. Wong, J. L. Andres, M. Head-Gordon, E. S. Replogle, and J. A. Pople, GAUSSIAN 98 (Revision A.11) (Gaussian, Inc., Pittsburgh, PA, 1998).
[19] M. Dolg, U. Wedig, H. Stoll, and H. Preuss, J. Chem. Phys. **86**, 866 (1987); D. Andrae, U. Häussermann, M. Dolg, H. Stoll, and H. Preuss, Theor. Chim. Acta **77**, 123 (1990).
[20] A. Bergner, M. Dolg, W. Küchle, H. Stoll, and H. Preuss, Mol. Phys. **80**, 1431 (1993).
[21] G. V. Girichev, V. M. Petrov, N. I. Giricheva, and K. S. Krasnov, Zh. Strukt. Khim. **23**, 56 (1982) [J. Struct. Chem. **23**, 45 (1982)].
[22] Y. Morino and H. Uehara, J. Chem. Phys. **45**, 4543 (1966).
[23] G. V. Girichev, N. I. Giricheva, and T. N. Malysheva, Zh. Fiz. Khim. **56**, 1833 (1982).
[24] T. Helgaker, H. J. Aa. Jensen, P. Jørgensen, J. Olsen, K. Ruud, H. Ågren, A. A. Auer, K. L. Bak, V. Bakken, O. Christiansen, S. Coriani, P. Dahle, E. K. Dalskov, T. Enevoldsen, B. Fernandez, C. Hättig, K. Hald, A. Halkier, H. Heiberg, H. Hettema, D. Jonsson, S. Kirpekar, R. Kobayashi, H. Koch, K. V. Mikkelsen, P. Norman, M. J. Packer, T. B. Pedersen, T. A. Ruden, A. Sanchez, T. Saue, S. P. A. Sauer, B. Schimmelpfennig, K. O. Sylvester-Hvid, P. R. Taylor, and O. Vahtras, DALTON, a molecular electronic structure program, Release 2.0 (2003).
[25] P. Pyykkö, Mol. Phys. **99**, 1617 (2001); *CRC Handbook of Chemistry and Physics*, 83rd ed., edited by D. R. Lide (CRC Press, Boca Raton, FL, 2002).
[26] P. Raghavan, At. Data Nucl. Data Tables **2**, 189 (1989).
[27] W. Kutzelnigg, U. Fleischer, and M. Schindler, in *NMR Basic Principles and Progress*, edited by P. Diehl, E. Fluck, H. Günther, R. Kosfeld, and J. Seelig (Springer-Verlag,Berlin, 1990), Vol. 23.
[28] T. H. Dunning, Jr., J. Chem. Phys. **90**, 1007 (1989).
[29] D. E. Woon and T. H. Dunning, Jr., J. Chem. Phys. **98**, 1358 (1993).
[30] A. K. Wilson, D. E. Woon, K. A. Peterson, and T. H. Dunning, Jr., J. Chem. Phys. **110**, 7667 (1999).
[31] S. Huzinaga, *Approximate Atomic Functions* (University of Alberta, Edmonton, 1971).
[32] K. Fægri, Jr. (private communication). See also http://folk.uio.no/knutf/bases/one.
[33] K. Eichkorn, F. Weigend, O. Treutler, and R. Ahlrichs, Theor. Chem. Acc. **97**, 119 (1997).
[34] A. D. Becke, J. Chem. Phys. **98**, 5648 (1993); P. J. Stephens, F. J. Devlin, C. F. Chabalowski, and M. J. Frisch, J. Phys. Chem. **98**, 11623 (1994).
[35] B. O. Roos, P. R. Taylor, and P. E. M. Siegbahn, Chem. Phys. **48**, 157 (1980).
[36] J. Olsen, B. O. Roos, P. Jørgensen, and H. J. Aa. Jensen, J. Chem. Phys. **89**, 2185 (1988); P.-Å. Malmqvist, A. Rendell, and B. O. Roos, J. Phys. Chem. **94**, 5477 (1990).
[37] J. Vaara, P. Manninen, and P. Lantto, in *Calculation of NMR and EPR Parameters: Theory and Applications*, edited by M. Kaupp, M. Bühl, and V. G. Malkin (Wiley-VCH, Weinheim, 2004).
[38] R. E. Wasylishen, Can. J. Chem. **62**, 981 (1984).